International Journal of Adhesion & Adhesives 44 (2013) 157–165

Contents lists available at SciVerse ScienceDirect

International Journal of Adhesion & Adhesives

journal homepage: www.elsevier.com/locate/ijadhadh

Fracture behavior of a self-healing, toughened epoxy adhesive

Henghua Jin [a,c], Gina M. Miller [a], Stephen J. Pety [b,c], Anthony S. Griffin [b,c], Dylan S. Stradley [b,c], Dennis Roach [d], Nancy R. Sottos [b,c], Scott R. White [a,c,*]

[a] Aerospace Engineering, University of Illinois at Urbana-Champaign Urbana, IL 61801, USA
[b] Materials Science and Engineering, University of Illinois at Urbana-Champaign, Urbana, IL 61801, USA
[c] Beckman Institute for Advanced Science and Technology, University of Illinois at Urbana Champaign, Urbana, IL 61801, USA
[d] FAA Airworthiness Assurance Center, Sandia National Laboratories, USA

ARTICLE INFO

Article history:
Accepted 12 February 2013
Available online 19 February 2013

Keywords:
Epoxy adhesive
Self-healing
Microcapsule
Fracture toughness

ABSTRACT

A self-healing, toughened epoxy adhesive is demonstrated based on a commercial structural adhesive film. Self-healing is achieved via embedded microcapsules containing dicyclopentadiene monomer and solid particles of bis(tricyclohexylphosphine)-benzylidine ruthenium (IV) dichloride (Grubbs') catalyst. Recovery of fracture toughness is assessed through fracture testing of width tapered double cantilever beam (WTDCB) specimens. Healing efficiencies as high as 58% were achieved for 6.6 wt% DCPD microcapsules and 10 mg Grubbs' catalyst. However, virgin fracture toughness is reduced with the addition of ca. 117 μm diameter microcapsules as a result of suppression of the damage zone as revealed by transmission optical micrographs. The uniform dispersal of microcapsules throughout a rubber toughened epoxy adhesive formulated using EPON 828, piperidine and CTBN alleviated the suppression effect and demonstrated retention of virgin fracture toughness of adhesives.

1. Introduction

Adhesive bonding reduces weight and complexity in the fabrication of many structural components, most notably in the aerospace industry. For example, sandwich panels formed by adhesively bonding composite skin panels to a low density (e.g. honeycomb) core yields structural panels with exceptional specific stiffness [1]. Adhesive bonding is also the primary method of repair of structural composites for scarf and doubler repairs [2]. Recently, composite doubler repairs have also been extended to aluminum and steel components [3,4] where a boron-epoxy composite patch is applied to the metal surface using an epoxy adhesive film. The composite doubler and the adhesive film are co-cured to effectively create a composite patch spanning the substrate crack. These patches extend the lifetime of the parent structure and eliminate or postpone the need for costly repairs.

Although adhesive bonding provides optimal load transfer and structural efficiency, adhesives have largely been relegated to secondary structures due to concerns about the fatigue and durability of bonded joints over their structural lifetime [5] and the difficulty of bondline inspection following manufacturing and during service [6]. Both concerns could be addressed by self-healing adhesives with extended service life and reduced inspection and maintenance. Building on previous work on the bulk healing of epoxy polymers, a self-healing epoxy adhesive was recently demonstrated that cures at room temperature and shows crack arrest under moderate fatigue loading conditions [7].

Unmodified epoxy adhesives are brittle and offer poor resistance to crack formation and propagation. Commercial epoxy adhesives are engineered for optimal toughness by incorporating phase-separated thermoplastics [8–10], rubber particles [11–14], or rigid inorganic particles [15–25]. Typically, they are cured at elevated temperature to increase strength and activate chemical bonding at the substrate/adhesive interface.

In this paper we demonstrate a self-healing rubber-toughened epoxy adhesive cured at elevated temperature based on the commercial system FM®73M (Cytec Engineered Materials). Self-healing is achieved with a microencapsulated healing agent and chemical catalyst dispersed in the adhesive matrix, an approach introduced by White et al. [26] for bulk polymer healing. While self-healing has been demonstrated for a variety of polymers and composites [27], self-healing adhesives are relatively unexplored. A significant challenge to their development is the seamless incorporation of self-healing components (e.g. microcapsules) into thin film adhesives. In addition, exposure to elevated temperature during curing of the adhesive places strict demands on the chemical and thermal stability of the healing chemistries employed. Here, we demonstrate autonomic healing and recovery of fracture toughness for a high temperature cured rubber-toughened epoxy adhesive of ca. 750 μm thickness.

* Corresponding author at: Aerospace Engineering, University of Illinois at Urbana-Champaign, Urbana, IL 61801 USA. Tel.: +1 217 333 1077.
E-mail address: swhite@illinois.edu (S.R. White).

0143-7496/$ - see front matter © 2013 Elsevier Ltd. All rights reserved.
http://dx.doi.org/10.1016/j.ijadhadh.2013.02.015

2. Experimental methods

2.1. Adhesive and self-healing system

The adhesive used in this study is FM®73M adhesive film supplied by Cytec Engineered Materials. FM®73M adhesive film is a general purpose aerospace epoxy adhesive film of 380 μm nominal thickness supported by a polyester mat. The film was cured in a programmable oven according to the temperature profile shown in Fig. 1a with a 3 h dwell at 110 °C.

The self-healing adhesive contains two components integrated with the FM®73M adhesive film. The first component is a microencapsulated liquid monomeric healing agent, *endo*-dicyclopentadiene (DCPD). DCPD has low viscosity and excellent shelf life when stabilized with 100–200 ppm *p-tert*-butylcatechol [28]. DCPD microcapsules with poly(urea-formaldehyde) (UF) shell walls [29] have been widely used in achieving self-healing for room temperature cured epoxy [30], vinyl polymers [31], and structural fiber-reinforced composites [32,33]. Thermogravimetric analysis (TGA) of this type of microcapsule shows 80% mass loss of core material after exposure to the cure cycle of FM®73M adhesive (Fig. 1b). In order to survive FM®73M's harsh curing conditions, a more thermally robust microcapsule must be employed and recent encapsulation research has led to the development of double-walled polyurethane (PU)–poly(UF) microcapsules [34] with significantly greater thermal stability as indicated in the TGA trace in Fig. 1b where total mass loss after the FM®73M adhesive cure cycle is ca. 8%. Double-walled microcapsules (Fig. 2a and b)

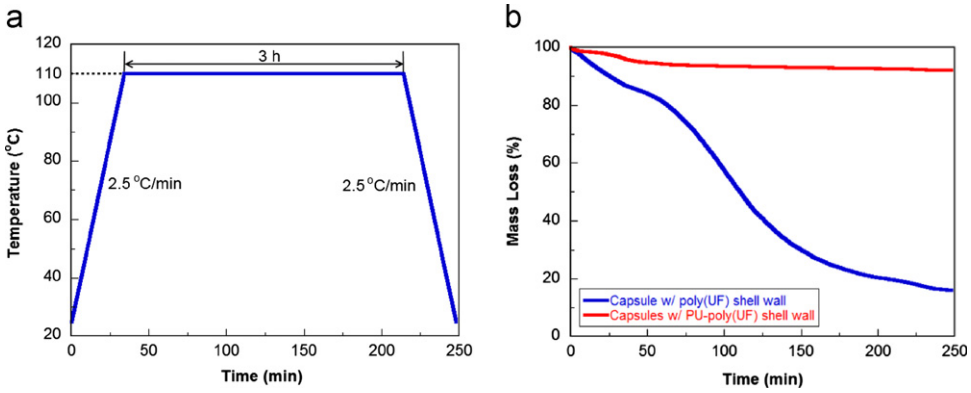

Fig. 1. Thermal characterization of adhesive system: (a) cure cycle used for FM®73M curing and (b) thermogravimetric analysis (TGA) of DCPD UF single wall microcapsules and PU/UF double shell wall microcapsules subject to the cure cycle from (a).

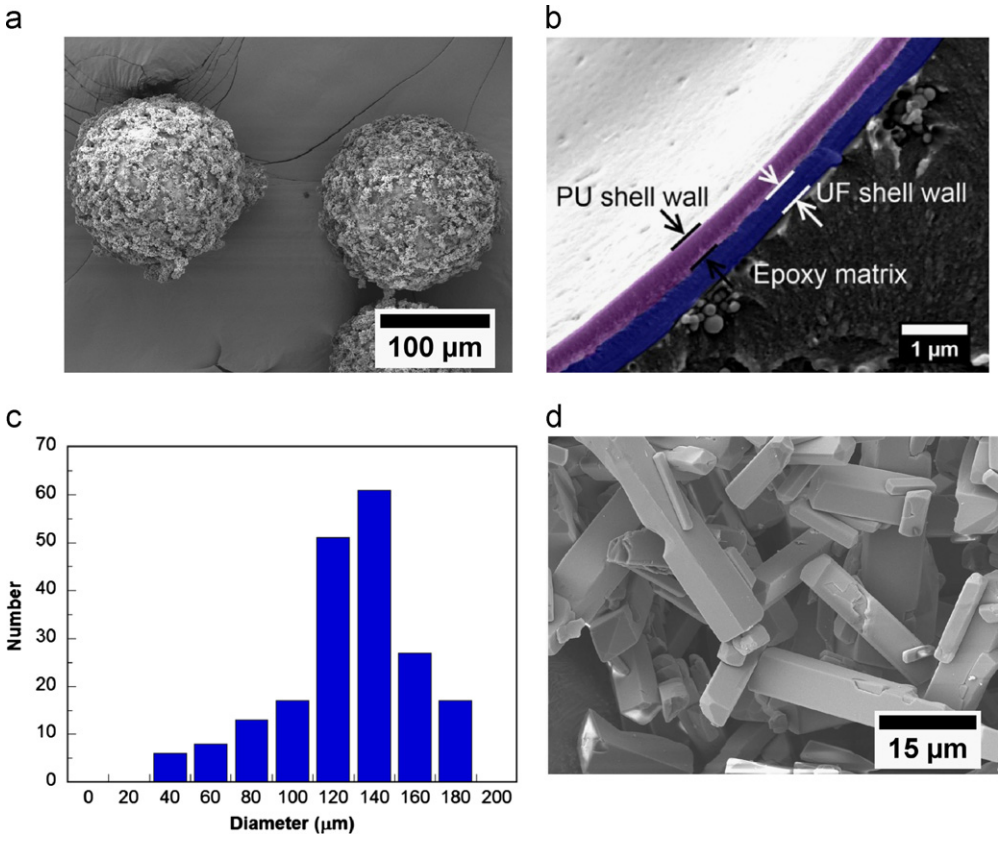

Fig. 2. Characterizations of healing components: (a) PU–UF double-walled DCPD microcapsules, (b) double shell wall with PU as internal shell wall and UF as outer shell wall, (c) size histogram of double-walled DCPD microcapsule used in this study, and (d) Grubbs' first generation catalyst particles (as-received).

containing DCPD core were prepared following a slightly modified encapsulation procedure as outlined in Fig. S1 (see Supporting Information). The microcapsules were air-dried and sieved to obtain capsules with diameters between 25 and 175 μm. A histogram of microcapsule diameter for microcapsules used in this study is shown in Fig. 2c which yields a mean diameter of 117 μm.

The second component of the self-healing system is bis(tricyclohexylphosphine)benzylidine ruthenium (IV) dichloride (first generation) Grubbs' catalyst particles (Fig. 2d). This catalyst was purchased from Sigma-Aldrich (Saint Louis, MO) and used as received. When mixed with DCPD monomer, Grubbs' catalyst initiates a ring-opening-metathesis-polymerization (ROMP) reaction resulting in a tough crosslinked polymer [26,28].

For control specimens hollow polymeric microcapsules were prepared by in situ polymerization of urea-formaldehyde pre-polymer [35]. The pre-polymer solution was first prepared by dissolving 10.25 g of urea into 27.5 g of formalin (37% formaldehyde in water) in a 150 mL beaker and allowing the reaction to proceed at 70 °C for 1 h. The pre-polymer solution was then added to a 500 mL beaker that contained 50 mL deionized H_2O and 12.55 mL 2.5 wt% EMA. The beaker was placed in a temperature-controlled water bath, and then agitated at 1200 rpm with a digital mixer (Eurostar, IKA Labortechnik) driving a three-bladed, 63.5 mm diameter low-shear mixing propeller (Cole Parmer). The propeller was placed just beneath the solution surface in order to entrap air bubbles. The water bath temperature was set to 35 °C with a ramp rate of 120 °C/h. When the bath temperature reached 30 °C, the pH was adjusted using formic acid to 2.0. Once the bath temperature reached 34 °C, 25 mL warm deionized water (~30 °C) was added. Thereafter, 15 mL of warm deionized water was added after an additional 15 and 30 min and 50 mL after 45 and 60 min. The water bath temperature was then set to 34 °C and the solution was allowed to react for 2 h.

Hollow microcapsules between 30 and 180 μm yielding an average diameter of 123 μm were sieved and collected. Glass beads (125–180 μm) were obtained from McMaster-Carr and used as a low profile additive (20 mg) to control adhesive bondline thickness. A 25 μm thick fluoropolymer release ply film (A4000R, Airtech International) was used to serve as a pre-crack during the specimen preparation. In order to integrate the two self-healing components with the FM®73M film adhesive, EPON™ 828 epoxy resin (Miller-Stephenson) was used as a carrier (liquid) phase for dispersion of self-healing components on the surface of the adhesive film. Silane coupling agent (3-

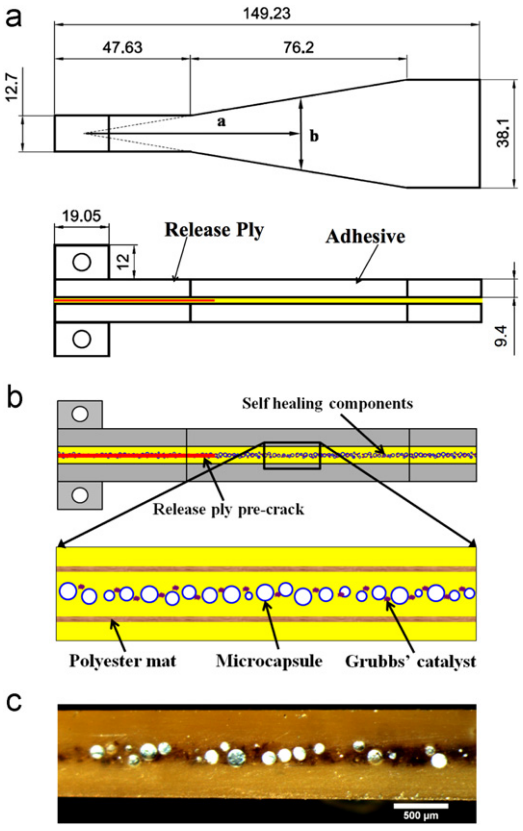

Fig. 3. Schematic of width tapered doubled cantilever beam (WTDCB) specimen: (a) dimensions of WTDCB specimen given in the units of mm, (b) schematic of WTDCB specimen with microcapsules and Grubbs' catalyst incorporated into the adhesive and (c) cross section of a self-healing specimen with 5 wt% DCPD microcapsules.

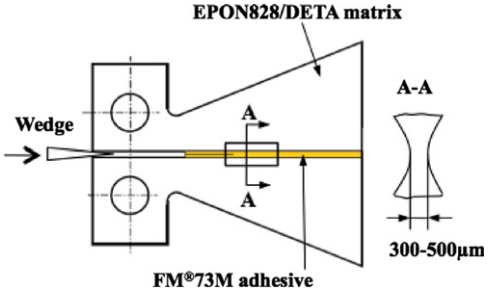

Fig. 4. Schematic of TDCB test specimen for transmission optical microscopy.

Table 1
Adhesive components for all WTDCB specimens. The amount of DCPD microcapsules incorporated into control type III and self-healing samples varied from 39 mg to 271 mg.

Specimen type	Adhesive components					
	FM®73M (mg)	EPON 828-silane mixture (mL)	DCPD capsule (mg)	Hollow capsule (mg)	Grubbs' catalyst (mg)	Glass bead (mg)
Control type I	3000	0.7	–	–	–	–
Control type II	3000	0.7	–	35	10	20
Control type III	3000	0.7	39–271	–	–	20
Self-healing	3000	0.7	39–271	–	10	20

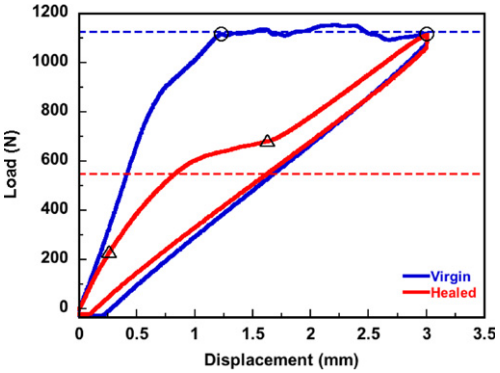

Fig. 5. Representative loading curves of virgin and healed tests of self-healing adhesive specimen with 5 wt% DCPD microcapsules and 10 mg Grubbs' first generation catalyst. Dashed lines represent the average critical loads for virgin and healed tests.

glycidyloxypropyl)trimethoxysilane was obtained from Sigma-Aldrich (and used to improve the adhesion of steel substrates and microcapsules to the epoxy adhesive). A36 structural steel was purchased from Speedy Metals (Rockford, IL) and used as the substrate material.

2.2. Characterization

Microcapsules were imaged using a Leica DMR Optical Microscope in transmission mode and images were processed using ImageJ software (version 1.42). A field emission environmental scanning electronic microscope (Philips XL30 ESEM-FEG) was used to image the fracture surfaces of specimens and microcapsules under high magnification. Fracture surfaces of interest were sputter-coated with ca. 30 nm thick layer of gold–palladium before imaging.

2.3. Specimen geometry

The width tapered double cantilever beam (WTDCB) specimen geometry was used in the present study (Fig. 3), following an established protocol for assessment of the fracture toughness and self-healing behavior of adhesively bonded steel substrates [7]. Linear elastic fracture mechanics analysis of the mode-I stress intensity factor for this specimen yields,

$$K_{Ic} = 2Pk\sqrt{\frac{3E_a}{(1-v_a^2)E_s h_s^3}}, \quad (1)$$

where P is the applied load, k is the taper ratio (for this study, $k=3$ is used), v_a is the adhesive Poisson's ratio (0.35) [36], h_s is the substrate thickness (9.4 mm), and E_a and E_s are the modulus of elasticity of the adhesive (2.27 GPa) [36] and the substrate (200 GPa), respectively. The healing efficiency (η) is defined as the ratio of the healed fracture toughness to the virgin fracture toughness [30] and for the WTDCB geometry, this reduces to the ratio of critical fracture loads, i.e.

$$\eta = \frac{K_{IC}^{healed}}{K_{IC}^{virgin}} = \frac{P_c^{healed}}{P_c^{virgin}} \quad (2)$$

2.4. Specimen types and preparation

Steel adherends were prepared for bonding by manual sanding using 80 grit sandpaper and cleaning with compressed air and acetone, followed by wiping to remove debris from the surface. Adherends were then rinsed with 1 vol% silane coupling agent in deionized water, dried at room temperature for 30 min, then placed in a 60 °C oven for 1 h.

WTDCB specimens were fabricated by first cutting the adhesive film to shape and placing one layer on each adherend surface. Next, a mixture of the carrier liquid (EPON 828) and various additional components (depending on the specimen type) was prepared, degassed, and then spread onto each film surface. A 25 μm release ply film was placed on the surface of one adherend to serve as a pre-crack. The two adherends were then aligned and pressure applied by elastic bands on both ends of the sample. The specimens were then placed in a programmable oven and cured according to the cure cycle in Fig. 1a.

Three types of control specimens were prepared along with the self-healing adhesive. The composition of the mixture included in the carrier liquid for each type is listed in Table 1. In each case, 0.7 mL of EPON 828 resin is combined with 1 wt%

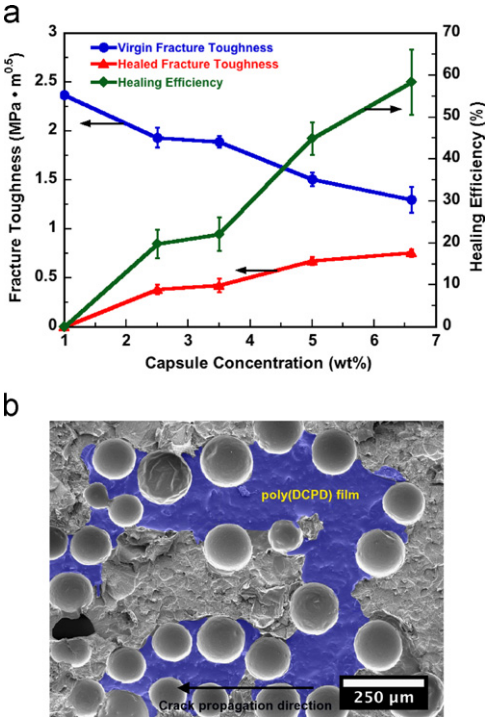

Fig. 6. Quasi-static fracture test results: (a) fracture toughness of virgin and healed tests, and healing efficiency for self-healing specimens as a function of microcapsule concentrations. (b) Scanning electron micrograph of fracture plane of a self-healing specimen with 5 wt% microcapsules with poly(DCPD) film outlined.

Table 2
Fracture toughness and healing efficiency of control and self-healing specimens.

Specimen type	No. of specimen	Capsule fraction (wt%)	Capsule mass (mg)	K_{Ic}^{Virgin} ($MPa \cdot m^{1/2}$)	K_{Ic}^{Healed} ($MPa \cdot m^{1/2}$)	Healing efficiency (%)	Adhesive thickness (μm)
Control type I	5	0	0	2.63 ± 0.08	0.72 ± 0.04	28 ± 2	719 ± 12
Control type II	4	–	35	1.49 ± 0.03	0.66 ± 0.05	44 ± 4	780 ± 12
Control type III	4	1	39	2.61 ± 0.08	–	–	767 ± 9
Control type III	4	2.5	98	2.30 ± 0.08	–	–	767 ± 8
Control type III	4	3.5	139	2.11 ± 0.07	–	–	765 ± 7
Control type III	5	5.0	201	1.95 ± 0.05	–	–	780 ± 5
Control type III	5	6.6	271	1.72 ± 0.06	–	–	789 ± 23
Self-healing	5	1	39	2.37 ± 0.03	0	0	761 ± 12
Self-healing	4	2.5	98	1.93 ± 0.10	0.38 ± 0.05	20 ± 3	754 ± 11
Self-healing	6	3.5	139	1.89 ± 0.06	0.42 ± 0.07	22 ± 4	746 ± 9
Self-healing	5	5.0	201	1.51 ± 0.07	0.67 ± 0.04	45 ± 4	787 ± 3
Self-healing	5	6.6	271	1.30 ± 0.13	0.75 ± 0.04	58 ± 8	797 ± 10

silane coupling agent and degassed for 1 h before the addition of other components.

In order to examine the adhesive fracture behavior, transmission optical microscopy (TOM) was also performed. For this study a tapered double cantilever beam (TDCB) geometry [30] was used in order to allow imaging in through transmission (Fig. 4c). These specimens were manufactured with an epoxy substrate composed of EPON 828 cured with diethyltriamine (DETA) at 12 pph. The TDCB specimen was fractured along the center line groove and the two fracture planes were then sanded with 80 grit sandpaper. The sample was then bonded with FM®73M adhesive and cured using the same cure cycle as for the WTDCB specimens. After the curing was complete, an area approximately 10 mm ahead of the pre-crack tip was thinned to 300–500 μm, and polished sequentially with 300, 600, 1200 and 2400 grit sandpapers.

2.5. Testing procedure

Mode-I fracture tests for WTDCB specimens were performed using a MTS load frame (Instron 8500) with a 4000 N load cell in displacement control at a rate of 5 mm/min until reaching a prescribed crack opening displacement (δ_{max}). For control type I δ_{max} was 5 mm, while for control type II and self-healing specimens δ_{max} was 3 mm. For some control specimens (type I and II) manual injection of a healing solution was then performed while the specimen was held open under load. For control type I specimens a mixture of 0.5 mL DCPD and 2.5 mg Grubbs' catalyst was injected into the crack plane using a microliter syringe. For control type II specimens, 0.5 mL of DCPD monomer (no catalyst) was injected into the crack plane. After the initial (virgin) fracture test, the specimens were quickly unloaded to allow the fracture surfaces to come into contact and heal. After 24 h of healing at room temperature, the specimens were then reloaded until reaching the same δ_{max} of the corresponding virgin test. For TOM studies a wedge was utilized to open the TDCB specimen and propagate the crack (Fig. 4c).

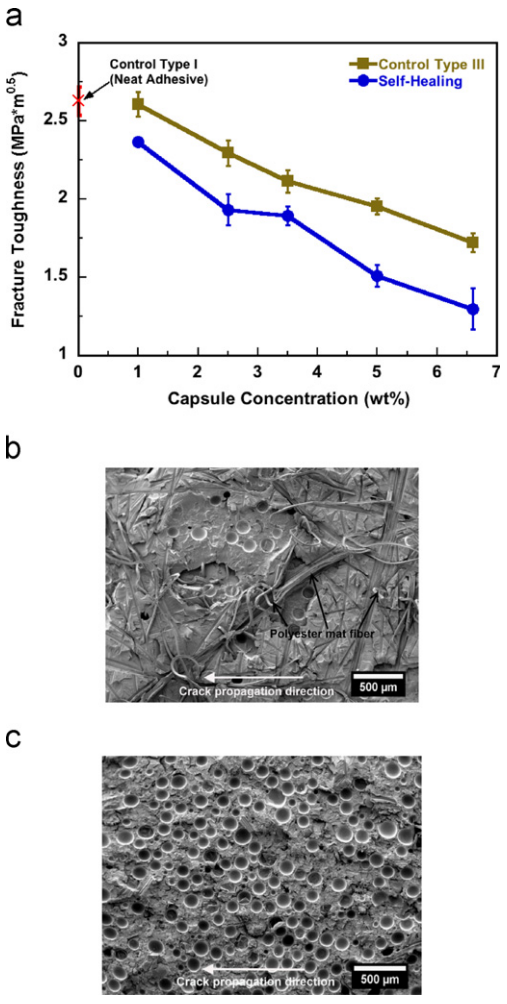

Fig. 7. (a) Fracture toughness of control type III specimens and self-healing specimens as a function of microcapsule concentrations. Fracture toughness of control type I (neat adhesive) specimen is included. (b) and (c) SEM micrographs of fracture plane of control type III specimens with 1.0 wt% and 5.0 wt% DCPD microcapsules, respectively.

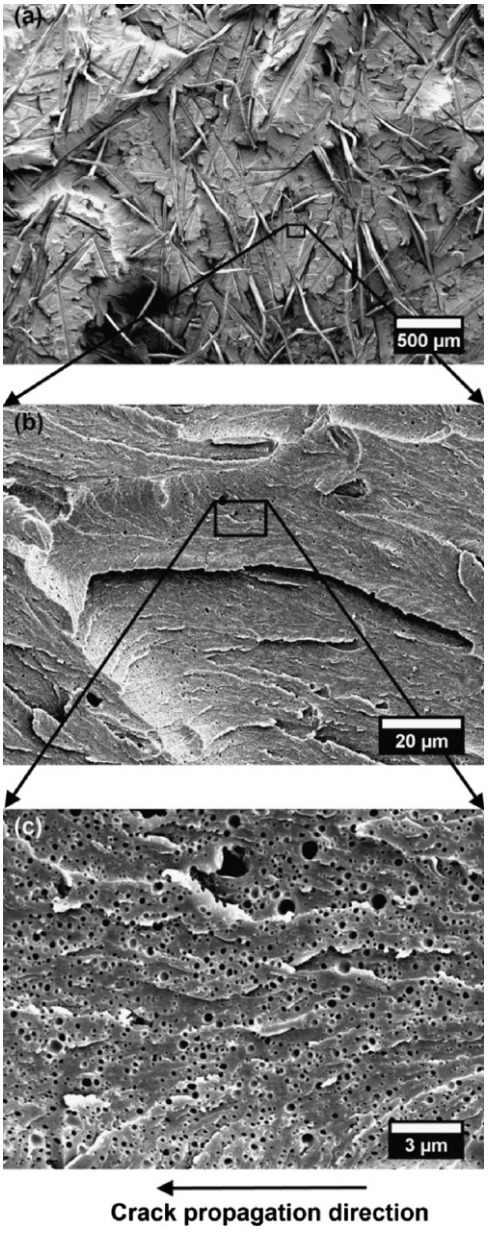

Fig. 8. Fracture morphology of control type I (neat epoxy) adhesive: (a) SEM micrograph of fracture plane showing significant out-of-plane morphology and polyester fiber debonding and fracture, (b) higher magnification image showing the secondary cracking and shear deformation of the matrix and (c) higher magnification image showing voids left after cavitation of (0.1–0.5 μm) rubber particles.

2.6. Data reduction

A typical test result for a self-healing specimen is shown in Fig. 5. In the virgin test, the loading curve is initially linear then becomes non-linear until the onset of stable crack propagation and a constant critical fracture load. For the healed test, the loading curve follows the virgin trace until crack propagation is reinitiated. Once the crack grows completely through the healed region the loading trace follows the slope of the unloading curve of the virgin test.

The average critical fracture load of the virgin test is calculated based on a sampling of all load values from the onset of crack propagation to the end of virgin crack propagation. The average healed critical load is calculated based on the mean value between the initiation and completion of crack propagation through the healed region. Crack initiation in the healed test was defined based on a 10% reduction in slope from that of the virgin test. Completion of fracture during the healed test occurs when the slope is within 10% of the virgin unloading stiffness. The average virgin critical load for this particular case is 1125 N and the average healed critical load is 549 N. As a consequence, the healing efficiency using Eq. (2) is $\eta = 48\%$. A similar data analysis procedure was used for all fracture tests conducted.

3. Experimental results

3.1. Control specimens

Three separate types of controls were tested in order to isolate various effects related to self-healing behavior and adhesive performance (Table 1). Control type I samples contained no self-healing components, but did incorporate the same amount of carrier fluid (epoxy) during specimen fabrication. Control type II samples contained the catalyst phase and hollow microcapsules while control type III samples contained the DCPD microcapsules only. Table 2 contains a summary of all WTDCB specimen test results.

Healing of type I controls was achieved by manual injection of a pre-mixed solution of DCPD monomer and Grubbs' catalyst. Type II controls were healed by manual injection of the DCPD monomer only since the catalyst phase was already incorporated within the adhesive. These "self-activated" controls remove the variable of monomer delivery to the crack plane via embedded microcapsules and they provide evidence of catalyst survival of the initial curing conditions. Healing efficiency of type I controls is 27.5% while that for type II controls is 44.4%. However, in both cases the healed fracture toughness is nearly the same and the discrepancy in healing efficiency is due to a reduction in virgin fracture toughness for type II controls. The healing data for type II specimens confirms that the catalyst phase is fully active after the adhesive curing cycle.

3.2. Self-healing specimens

Self-healing specimens contained both healing components in a fully integrated system. Fig. 6a presents the results of a series of tests in which the microcapsule concentration was varied from 1.0 to 6.6 wt%. For the smallest capsule concentration tested (1.0 wt%) no healing was detected indicating that insufficient healing agent was supplied to the crack plane. As the capsules concentration is increased, the healed fracture toughness increases and approaches a plateau beyond about 5 wt%. The healed fracture toughness for specimens containing 6.6 wt% capsules is the same as control type I specimens, indicating the healing agent released from the embedded microcapsules is sufficient to completely fill the crack plane.

4. Discussion

Examination of the healed fracture plane of a self-healing specimen by scanning electron microscopy (Fig. 6b) reveals evidence of microcapsule rupture and polyDCPD film formation

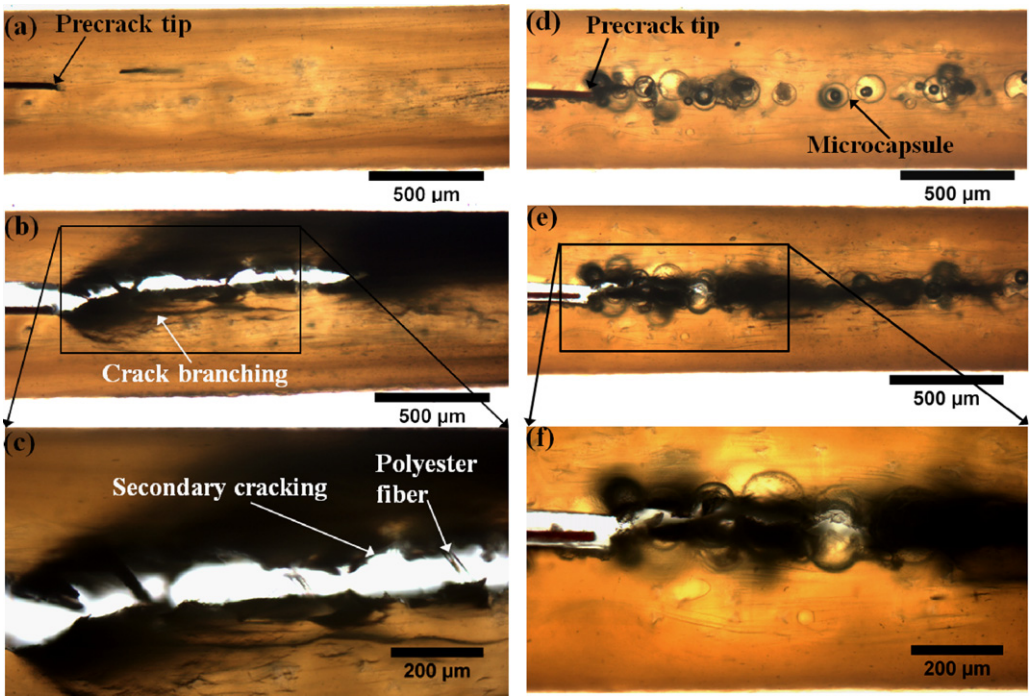

Fig. 9. Transmission optical microscopy (TOM) of neat epoxy (control type I) and microcapsule-only (control type III) adhesive during fracture. TOM of TDCB fracture of control type I specimen (a)–(c): (a) before crack growth, (b) after crack growth, showing the damage zone at the crack tip, (c) higher magnification showing the secondary cracking and fiber bridging. TOM of TDCB fracture of control type III specimen (d)–(f): (d) before crack growth, (e) after crack growth, showing the damage zone at the crack tip, and (f) higher magnification of (e).

by the in situ reaction of DCPD and Grubbs' catalyst. The maximum healing efficiency achieved is 58 ± 8% for specimens containing 6.6 wt% capsules. However, increased healing efficiency occurs at the expense of virgin fracture toughness which continuously decreases with increasing microcapsule concentration. Nevertheless, self-healing is achieved for a toughened adhesive cured at elevated temperature (110 °C for 3 h), an important technical advancement for self-healing polymers.

While the virgin fracture toughness of FM®73M self-healing adhesive decreases as the concentration of microcapsule increases, this reduction is counter to that observed for an untoughened self-healing epoxy adhesive [7] and bulk polymers like epoxy [37], vinyl ester [31], and PDMS [38]. Two operative toughening phenomena have been identified for embedded microcapsules related to crack pinning and localized plastic deformation [37]. However, crack tails or steps, which are typical features of crack pinning, are not observed in the present self-healing adhesive system upon inspection of fracture surfaces.

To better understand the observed effects, we prepared and tested a series of control type III specimens (DCPD microcapsules only). A similar trend was observed in type III controls in which the virgin toughness monotonically decreased with increasing capsule concentration (Fig. 7a). These controls were devoid of poly(DCPD) on the fracture plane (due to the absence of Grubbs' catalyst) and allowed direct examination of the fracture plane. As shown in Fig. 7b and c, the morphology of the fracture plane was significantly altered at higher capsule concentration.

More detailed examination of the fracture surfaces on control type I samples (Fig. 8) reveals large shear deformation of the epoxy matrix and permanently dilated cavities between 0.1–0.5 μm in the native adhesive system. These features are commonly observed in rubber-toughened epoxy systems [13,39,40]. Fig. 8 also contains evidence of secondary toughening mechanisms associated with deformation and fracture of the polyester supporting mat such as fiber debonding, fiber bridging and crack branching [41–43]. In contrast, the self-healing adhesive specimens show no evidence of these secondary mechanisms on the fracture plane as the microcapsule concentration increases (Fig. 7c).

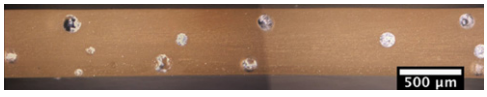

Fig. 10. Cross sectional optical image of adhesive formulated with EPON 828/piperidine/CTBN containing 5 wt% DCPD microcapsules showing uniform dispersion of microcapsules.

To further investigate the influence of microcapsules on fracture toughness, transmission optical micrographs (TOM) were taken during crack propagation near the crack tip in thin TDCB specimens. A control type I specimen is compared directly to a control type III adhesive specimen with 5 wt% microcapsules in Fig. 9. Internal cavitation of rubber particles and shear band formation suppress light transmission in the damage zone [39,40]. The type I control specimen has a large damage zone as well as crack bridging from the polyester mat. The type III control specimen develops a much smaller damage zone and the fracture process remains localized in the middle of the adhesive layer.

The suppression of the damage zone in adhesives with embedded microcapsules is likely the result of stress concentrations associated with the microcapsules localized on the center line of the adhesive. The stress field due to microcapsules interacts with the crack tip stress field, raising the local stresses between the crack tip and the capsule. This interaction can lead to cavitation of rubber particles in the vicinity and subsequent shear yielding of the matrix [39,40]. Since the capsules are only present in the center of the adhesive, the damage is localized to that region alone, suppressing cavitation and attendant shear deformations away from the central region of the adhesive as well as secondary toughening effects like fiber fracture, fiber debonding, and crack branching from the polyester fiber mat.

Localization of damage could be avoided by dispersing microcapsules throughout the entire adhesive region. To demonstrate this concept, a rubber-toughened epoxy adhesive was formulated using EPON 828 resin, piperidine curing agent, and CTBN liquid rubber [40]. DCPD microcapsules were incorporated uniformly throughout the adhesive layer (Fig. 10, see Supporting Information

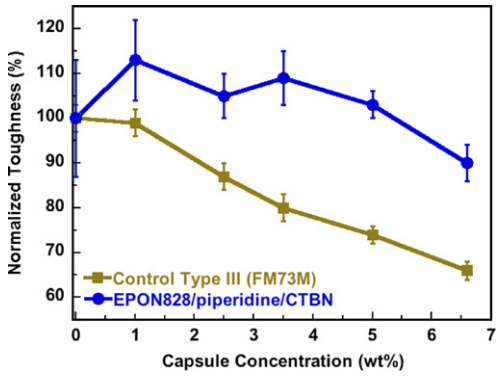

Fig. 12. Normalized fracture toughness ($K_{IC}/K_{IC,\ neat}$) of EPON 828/piperidine/CTBN epoxy adhesive specimens as a function of microcapsule concentration compared with control type III specimens.

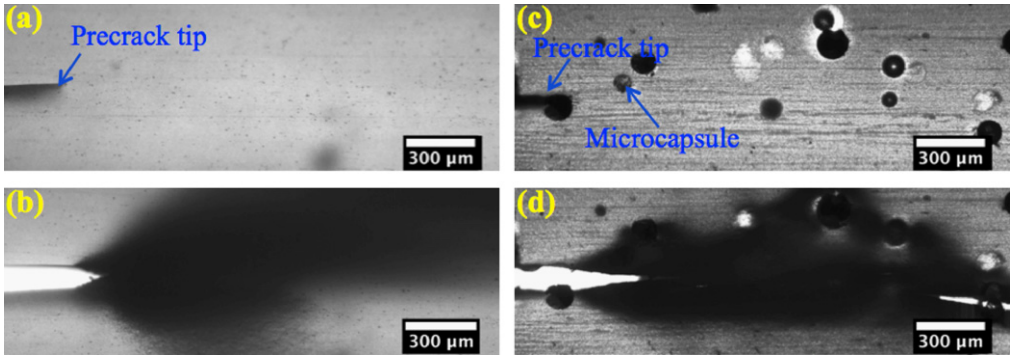

Fig. 11. TOM of neat epoxy and capsule-containing epoxy formulated using EPON 828, piperidine and CTBN during fracture. TOM of TDCB fracture of neat epoxy specimen: (a) before crack growth, (b) after crack growth, showing the damage zone at the crack tip. TOM of TDCB fracture of epoxy specimen containing 5 wt% DCPD capsules: (c) before crack growth, (d) after crack growth, showing the damage zone at the crack tip.

for sample preparation procedure). TOM studies of fracture behavior of this type of epoxy were also conducted in thin TDCB specimens. As revealed in Fig. 11, upon crack propagation, a large plastic zone was observed in epoxy containing 5 wt% DCPD microcapsules comparable to that in the corresponding neat case. Fracture tests on WTDCB samples made with these adhesives (ca. 540 μm thickness) demonstrated an improvement in virgin fracture toughness with up to 6.6 wt% microcapsule concentration (Fig. 12). The enhancement of toughness is largely attributed to damage zone branching caused by stress field interactions between the microcapsules and the crack tip [39,40]. SEM images of the fracture plane of a specimen containing 5 wt% microcapsules (Fig. 13) reveal a very rough fracture surface with ruptured microcapsules and cavitation of rubber particles. The extensive out-of-plane fracture and large shear deformation indicate crack branching was operative during fracture. This fracture surface is significantly different than the relatively flat fracture plane of the FM-73M control type III sample containing 5 wt% microcapsules in Fig. 7c.

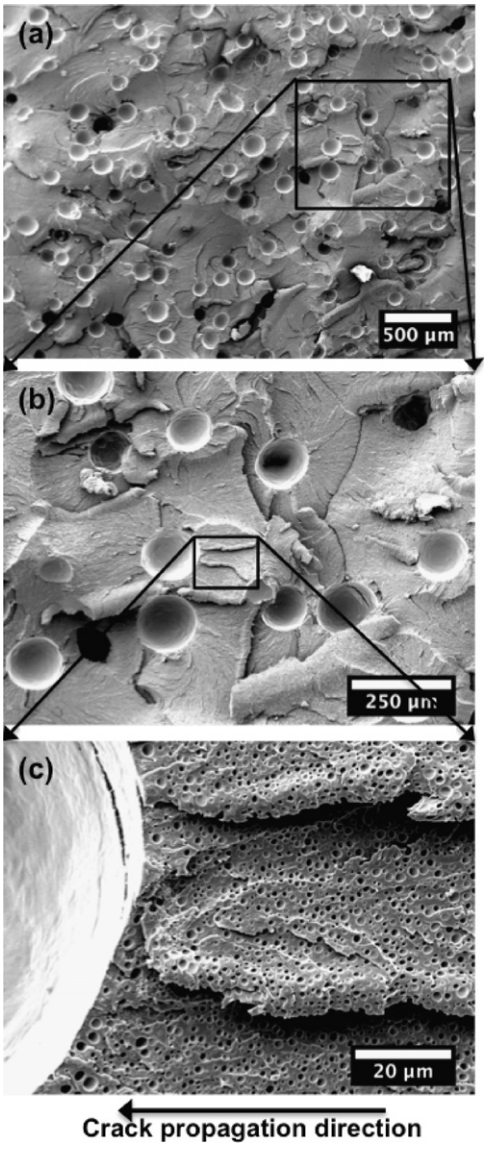

Fig. 13. SEM micrographs of fracture plane of EPON 828/piperidine/CTBN adhesive specimens containing 5 wt% DCPD microcapsules: (a) SEM micrograph of fracture plane showing rough texture morphology, (b) higher magnification image showing out-of-plane cracking and shear deformation of the matrix and (c) higher magnification image revealing voids left after cavitation of CTBN rubber particles.

Utilizing smaller diameter capsules closer in size to the rubber particles (0.1–0.5 μm) would also facilitate a more homogeneous dispersion. Methods have been developed to produce submicron capsules and disperse them in epoxy matrices to provide enhanced toughness [44]. Since the volume of healing agent delivered to the fracture plane scales linearly with capsule diameter [45], optimization of capsule size and concentration for improved toughening and high healing efficiency is critical for future development of self-healing, toughened epoxy adhesives.

5. Conclusion

A self-healing rubber toughened structural adhesive based on the commercial system FM®73M has been developed by incorporating microcapsules containing DCPD monomer and particles of Grubbs' catalyst. Recovery of quasi-static mode-I fracture toughness was assessed using WTDCB test specimens. Healing efficiency based on the recovery of virgin fracture toughness ranged from 20% to 58% and increased with microcapsule concentration. Importantly, self-healing was demonstrated for an epoxy adhesive subjected to high temperature curing (110 °C, 3 h), an significant technical advancement in self-healing polymers.

The addition of 117 μm average diameter microcapsules into ca. 750 μm thick adhesives was shown to reduce the virgin fracture toughness with increasing microcapsule concentration. This reduction in toughness was attributed to localization of the fracture to the center of the adhesive and a reduction in damage zone size. Uniform dispersion of microcapsules in a non-commercial rubber toughened adhesive effectively alleviated localization of damage and retained virgin fracture toughness.

Acknowledgments

The authors acknowledge funding support from the National Science Foundation (Grant # CMS 05-27965) and Sandia National Laboratories (BPO 378467). Stephen Pety was supported in part by an NDSEG fellowship, which is sponsored by the Department of Defense. In addition, the authors greatly acknowledge Dr. Chris Mangun and Dr. Mary M. Caruso for technical help and discussion. Manufacturing test specimens was accomplished with the help of Kent Elam in the Aerospace Engineering Machine Shop. Fracture testing was completed at the Advanced Materials Testing and Engineering Lab, with assistance of Peter Kurath, Gavin Horn and Rick Rottet. Electron microscopy was performed in the Imaging Technology Group of the Beckman Institute for Advanced Science and Technology, with the assistance of Scott Robinson.

Appendix A. Supporting information

Supplementary data associated with this article can be found in the online version at: http://dx.doi.org/10.1016/j.ijadhadh.2013.02.015.

References

[1] Kinloch AJ. Adhesives in engineering. Proc Inst Mech Eng G-J Aerosp Eng 1997;211:307–35.
[2] Baker AA, Rose LRF, Jones R. Advances in the bonded composite repair of metallic aircraft structure. Elsevier; 2002.
[3] Roach D, DeLong W, Rackow K, Yepez E, Reedy D, White SR. Use of composite materials, health monitoring, and self-healing concepts to refurbish our civil and military infrastructure. SAND report 2007-5547. Sandia National Lab; 2007.

[4] Roach D, Rackow K. Development of bonded composite doublers for the repair of oil recovery equipment. SAND2005-3195. Sandia National Lab; 2005.
[5] Jethwa JK, Kinloch AJ. The fatigue and durability behaviour of automotive adhesives. Part I: Fracture mechanics tests. J Adhes 1997;61:71–95.
[6] Hart-Smith LJ. A peel-type durability test coupon to assess interfaces in bonded, co-bonded, and co-cured composite structures. Int J Adhes Adhes 1999;19:181–91.
[7] Jin H, Miller GM, Sottos NR, White SR. Fracture and fatigue response of a self-healing epoxy adhesive. Polymer 2011;52:1628–34.
[8] Bucknall CB, Partridge IK. Phase-separation in epoxy-resins containing polyethersulfone. Polymer 1983;24:639–44.
[9] Kinloch AJ, Yuen ML, Jenkins SD. Thermoplastic-toughened epoxy polymers. J Mater Sci 1994;29:3781–90.
[10] Pascault JP, Williams RJJ. Formulation and characterization of thermoset–thermoplastic blends. In: Paul DR, Bucknall CB, editors. Polymer blends. New York: John Wiley & Sons; 1999. p. 379–415.
[11] Drake RS, Siebert AR. Elastomer-modified epoxy resins for structural applications. SAMPE Q 1975;6:11–21.
[12] Kinloch AJ. Toughening epoxy adhesives to meet today's challenges. MRS Bull 2003;28:445–8.
[13] Kinloch AJ, Shaw SJ, Tod DA, Hunston DL. Deformation and fracture-behavior of a rubber-toughened epoxy.1. Microstructure and fracture studies. Polymer 1983;24:1341–54.
[14] Pearson RA, Yee AF. Toughening mechanisms in elastomer-modified epoxies.2. Microscopy studies. J Mater Sci 1986;21:2475–88.
[15] Amdouni N, Sautereau H, Gerard JF. Epoxy composites based on glass-beads.2. mechanical-properties. J Appl Polym Sci 1992;46:1723–35.
[16] Johnsen BB, Kinloch AJ, Mohammed RD, Taylor AC, Sprenger S. Toughening mechanisms of nanoparticle-modified epoxy polymers. Polymer 2007;48:530–41.
[17] Kawaguchi T, Pearson RA. The effect of particle-matrix adhesion on the mechanical behavior of glass filled epoxies. Part 2. A study on fracture toughness. Polymer 2003;44:4239–47.
[18] Kinloch AJ, Lee JH, Taylor AC, Sprenger S, Eger C, Egan D. Toughening structural adhesives via nano- and micro-phase inclusions. J Adhes 2003;79:867–73.
[19] Kinloch AJ, Mohammed RD, Taylor AC, Eger C, Sprenger S, Egan D. The effect of silica nano particles and rubber particles on the toughness of multiphase thermosetting epoxy polymers. J Mater Sci 2005;40:5083–6.
[20] Kitey R, Tippur HV. Role of particle size and filler-matrix adhesion on dynamic fracture of glass-filled epoxy. II. Linkage between macro- and micro-measurements. Acta Mater 2005;53:1167–78.
[21] Lee J, Yee AF. Fracture of glass bead/epoxy composites: on micro-mechanical deformations. Polymer 2000;41:8363–73.
[22] Ragosta G, Abbate M, Musto P, Scarinzi G, Mascia L. Epoxy-silica particulate nanocomposites: chemical interactions, reinforcement and fracture toughness. Polymer 2005;46:10506–16.
[23] Spanoudakis J, Young RJ. Crack-propagation in a glass particle-filled epoxy-resin.1. Effect of particle-volume fraction and size. J Mater Sci 1984;19:473–86.
[24] Young RJ, Beaumont PWR. Failure of brittle polymers by slow crack growth.2. Failure processes in a silica particle filled epoxy-resin composite. J Mater Sci 1975;10:1343–50.
[25] Zhang H, Zhang Z, Friedrich K, Eger C. Property improvements of in situ epoxy nanocomposites with reduced interparticle distance at high nanosilica content. Acta Mater 2006;54:1833–42.
[26] White SR, Sottos NR, Geubelle PH, Moore JS, Kessler MR, Sriram SR, et al. Autonomic healing of polymer composites. Nature 2001;409:794–7.
[27] Blaiszik BJ, Kramer SLB, Olugebefola SC, Moore JS, Sottos NR, White SR. Self-healing polymers and composites. Annu Rev Mater Res 2010;40:179–211.
[28] Kessler MR, White SR. Cure kinetics of the ring-opening metathesis polymerization of dicyclopentadiene. J Polym Sci Polym Chem 2002;40:2373–83.
[29] Brown EN, Kessler MR, Sottos NR, White SR. In situ poly(urea–formaldehyde) microencapsulation of dicyclopentadiene. J Microencapsul 2003;20:719–30.
[30] Brown EN, Sottos NR, White SR. Fracture testing of a self-healing polymer composite. Exp Mech 2002;42:372–9.
[31] Wilson GO, Moore JS, White SR, Sottos NR, Andersson HM. Autonomic healing of epoxy vinyl esters via ring opening metathesis polymerization. Adv Funct Mater 2008;18:44–52.
[32] Kessler MR, Sottos NR, White SR. Self-healing structural composite materials. Compos Part A-Appl Sci Manuf 2003;34:743–53.
[33] Patel AJ, Sottos NR, Wetzel ED, White SR. Autonomic healing of low-velocity impact damage in fiber-reinforced composites. Compos Part A-Appl Sci Manuf 2010;41:360–8.
[34] Caruso MM, Blaiszik BJ, Jin HH, Schelkopf SR, Stradley DS, Sottos NR, et al. Robust, double-walled microcapsules for self-healing polymeric materials. ACS Appl Mater Int 2010;2:1195–9.
[35] Jin HH, Mangun CL, Stradley DS, Moore JS, Sottos NR, White SR. Self-healing thermoset using encapsulated epoxy-amine healing chemistry. Polymer 2012;53:581–7.
[36] Aydin MD, Ozel A, Temiz S. The effect of adherend thickness on the failure of adhesively-bonded single-lap joints. J Adhes Sci Technol 2005;19:705–18.
[37] Brown EN, White SR, Sottos NR. Microcapsule induced toughening in a self-healing polymer composite. J Mater Sci 2004;39:1703–10.
[38] Keller MW, White SR, Sottos NR. A self-healing poly(dimethyl siloxane) elastomer. Adv Funct Mater 2007;17:2399–404.
[39] Bagheri R, Williams MA, Pearson RA. Use of surface modified recycled rubber particles for toughening of epoxy polymers. Polym Eng Sci 1997;37:245–51.
[40] Pearson RA, Yee AF. Influence of particle-size and particle-size distribution on toughening mechanisms in rubber-modified epoxies. J Mater Sci 1991;26:3828–44.
[41] Choi NS, Takahashi K. Stress-fields on and beneath the surface of short-fiber-reinforced composites and their failure mechanisms. Compos Sci Technol 1992;43:237–44.
[42] Choi NS, Takahashi K. Toughness and microscopic fracture mechanisms of unfilled and short-glass-fibre-filled poly(cyano arylether). J Mater Sci 1996;31:731–40.
[43] Norman DA, Robertson RE. The effect of fiber orientation on the toughening of short fiber-reinforced polymers. J Appl Polym Sci 2003;90:2740–51.
[44] Blaiszik BJ, Sottos NR, White SR. Nanocapsules for self-healing materials. Compos Sci Technol 2008;68:978–86.
[45] Rule JD, Sottos NR, White SR. Effect of microcapsule size on the performance of self-healing polymers. Polymer 2007;48:3520–9.